Heliyon 10 (2024) e34661

Contents lists available at ScienceDirect

Heliyon

journal homepage: www.cell.com/heliyon

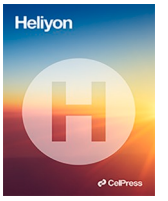

Research article

Study on the adsorption performance of fly ash loaded on nano-FeS for chromium-containing wastewater treatment

Xuying Guo [a,b,*], Zilong Zhao [b], Xinle Gao [b], Honglei Fu [c], Zhiyong Hu [b], Xiaoyue Zhang [c], Yanrong Dong [c]

[a] College of Science, Liaoning Technical University, Fuxin, 123000, Liaoning, China
[b] College of Mining, Liaoning Technical University, Fuxin, 123000, Liaoning, China
[c] College of Civil Engineering, Liaoning Technical University, Fuxin, 123000, Liaoning, China

ARTICLE INFO

Keywords:
Fly ash
Load
Nano-FeS
Chromium-containing wastewater
Adsorption performance

ABSTRACT

In view of the problems caused by chromium-containing wastewater, such as environmental pollution, biological toxicity, and human health risks. Based on fly ash adsorption and nano-FeS reduction characteristics, fly ash loaded nano-FeS composite (nFeS-FA) was synthesized using mineral supported modification technology and ultrasonic precipitation method. The effect of adsorbent dosage, initial pH, contact time, and initial concentration of the solution on the adsorption of Cr(VI) and total Cr by nFeS-FA was investigated. The characteristics of Cr(VI) and total Cr adsorption by nFeS-FA were studied using adsorption isotherms, adsorption kinetics principles, as well as XRD, TEM, SEM-EDS, and BET analysis. The results demonstrated that under the conditions of nFeS-FA of 8 g/L, initial pH of 4, contact time of 150 min, and initial concentration of the solution at 100 mg/L, nFeS-FA achieved removal efficiency of 87.85 % for Cr(VI) and 71.77 % for total Cr. The adsorption of Cr(VI) and total Cr by nFeS-FA followed the Langmuir model and pseudo-second-order kinetic model, indicating monolayer adsorption with chemical adsorption as the dominant mechanism. XRD, TEM, SEM-EDS, and BET revealed that the flaky nano-FeS was uniformly distributed on the surface of fly ash, exhibiting good dispersion and thereby increasing the specific surface area. During the adsorption experiments, nFeS-FA reacted with Cr(VI), and the generated Fe^{3+} mainly existed as FeOOH precipitation, while S^{2-} reacted with Cr(III) to produce Cr_2S_3 precipitation. Therefore, nFeS-FA exhibited excellent adsorption performance towards Cr(VI) and total Cr. It can serve as a technological reference for the remediation of heavy metal chromium pollution in the field of water treatment.

1. Introduction

Currently, global industrialization continues to maintain a strong momentum, and the issue of chromium pollution is increasingly prominent. The irrational discharge of chromium-containing wastewater will bring environmental pollution, biological toxicity, human health risks and other issues [1–3]. Presently, the methods commonly employed for treatment include ion exchange [4], microbial method [5,6], and adsorption method [7–9]. But these methods suffer from the problems of low treatment efficiency and high process costs. Among them, the chemical precipitation method [10–12] mainly uses reducing substances to transform heavy

* Corresponding author. College of Science, Liaoning Technical University, Fuxin, 123000, Liaoning, China.
E-mail address: guoxuying@lntu.edu.cn (X. Guo).

https://doi.org/10.1016/j.heliyon.2024.e34661
Received 27 February 2024; Received in revised form 21 June 2024; Accepted 15 July 2024
Available online 16 July 2024

metal ions in wastewater into precipitation compounds. It is widely used in the field of chromium pollution remediation because of its easy operation and fast reaction rate. Common reducing agents include nano zero-valent iron, nano-FeS, $Na_2S_2O_5$, and so on [13–15].

The research group's previous study [16,17] showed that nano-FeS, as an effective water treatment material, possessed wide adaptability, strong reduction capability, and a large specific surface area, and can efficiently remove a variety of pollutants. Hu et al. [18] utilized in-situ synthesized nano-FeS by sulfate-reducing bacteria to treat wastewater containing Cr(VI). Under optimal conditions, the adsorption capacity for Cr(VI) was found to be 18.6 mg/L. Li et al. [19] prepared nano-FeS particles by homogeneous precipitation method and treated Cr(VI) in soil. Under optimal conditions, and the removal efficiency of Cr(VI) was up to 98 %. However, nano-FeS possesses a high surface energy, making it prone to oxidation and aggregation, which greatly affects their adsorption performance. Therefore, the modification of nanoparticles using the mineral loading technique has been proposed. Lu et al. [20] prepared modified diatomite-loaded FeS composite material to remove Cr(VI) by hydrothermal synthesis method, and the adsorption capacity for Cr(VI) can reach up to 141.6 mg/g under optimal conditions. Li [21] prepared kaolinite loaded nano-FeS composite material to remove Cr(VI). Under optimal conditions, the maximum adsorption capacity reached 399 mg/g, showing significant improvement compared to single FeS. The research group [22] synthesized a composite material by combining the mineral material lignite as a carrier with nano-FeS. This composite material effectively remediated chromium wastewater under acidic conditions. However, these mineral materials are expensive and difficult to apply on a large scale. Therefore, there is a need for further screening of inexpensive carrier materials.

Fly ash, as an industrial solid waste, possesses favorable physicochemical properties such as high strength, large specific surface area, and low bulk density. Currently, it is widely utilized as an adsorbent in the field of water treatment [23,24]. Wang et al. [25] performed mechanical and chemical treatment on fly ash to make zeolite for Cr(VI) adsorption. Under optimal conditions, the synthesized zeolite exhibited a higher adsorption capacity for Cr(VI) at 1.549 mg/g, surpassing the raw fly ash (0.803 mg/g). Deng et al. [26] carried out alkali modification on fly ash to adsorb Cr(VI), and the saturated adsorption capacity was only 5.9762 mg/g according to Langmuir isothermal equation. Since these modification measures did not significantly improve the adsorption activity of fly ash, an exploration into the resource utilization of fly ash was considered [27]. Relevant studies have shown that using composite materials prepared by using fly ash as a carrier to load other substances can effectively overcome the drawback of poor adsorption performance of fly ash alone. Hosseini Asl et al. [28] prepared a novel composite material by combining hydrous iron oxide/aluminum hydroxide and fly ash for Cr(VI) adsorption. Under optimal conditions, the maximum removal efficiency of Cr(VI) was 84.9 %. Therefore, cheap and stable fly ash can be considered as a carrier material loaded with nano-FeS to improve the remediation efficiency on chromium-containing wastewater.

This study proposed the use of mineral supported modification technology, as well as ultrasonic precipitation method, to prepare a composite adsorption material called fly ash loaded on nano-FeS (nFeS-FA). It was applied in the experimental research for the remediation of chromium-containing wastewater. The nFeS-FA effectively improved the removal capacity and removal efficiency of fly ash for chromium, and also provided surface carriers for nano-FeS, improving the mechanical strength and stability of nanomaterials while addressing the issue of nanoparticle agglomeration. Combined with adsorption isotherm, adsorption kinetics, XRD, TEM, SEM-EDS, and BET analyses, the excellent adsorption properties of nFeS-FA for chromium were demonstrated, offering a novel approach for the remediation of chromium-contaminated wastewater.

2. Materials and methods

2.1. Materials and reagents

Fly ash: Sourced from Fuxin City, Liaoning Province, China. It was subjected to sieving and then washed three times with deionized water. After drying at 378.15 K, it was set aside for further use. Table 1 shows its main chemical components. The reagents required for the experiments were as follows: Diphenylcarbonyldihydrazide, Acetone, H_2SO_4, H_3PO_4, HNO_3, NaOH, K_2CrO_4, Na_2S, $FeSO_4$(AR, Sinopharm Chemical Reagent Co., Ltd., Shanghai, China). The entire experimental process was conducted using deionized water.

Acidic chromium-containing wastewater: The water sample used in this experiment was a simulated acidic mine wastewater with pH = 4. The pH of the solution was adjusted using a concentration of 0.1 mol/L HNO_3 or 0.1 mol/L NaOH. When preparing the water sample, an appropriate amount of K_2CrO_4 was dissolved in deionized water to prepare a solution containing Cr(VI) with a concentration of 100 mg/L.

2.2. Experimental method

2.2.1. Preparation of nFeS-FA

4 g of pre-treated fly ash were weighed and added to 200 mL of Na_2S solution of a certain concentration, stirred with Magnetic stirrer (84–1, Suzhou Guohua Instrument Co., Ltd.) for 8 h, stood for 3–5 min, slowly poured out the Na_2S solution, fly ash particles

Table 1
The main chemical composition of fly ash.

Constituent	SiO_2	TiO_2	Al_2O_3	Fe_2O_3	MnO	MgO	CaO	Na_2O	K_2O	P_2O_5
Content (%)	67.10	0.12	19.74	3.35	0.34	2.87	4.00	1.08	1.30	0.10

were left to be used. At room temperature(298.15 K), the conical bottle was placed in the ultrasonic environment, and $FeSO_4$ solution was dripped with peristaltic pump (F01A-STP, KAMOER Fluid Tech (Shanghai) Co., Ltd.) and mechanical agitator (LC-OES-150FR, Shanghai Lichen Instrument Technology Co., Ltd.) at the speed of 350 rpm. Then the frequency of ultrasonic cleaner (YM-031S, Shandong Jiajing Medical Technology Co., Ltd.) was controlled to 40 kHz and processed for 10 min. The suspension was removed and placed in a benchtop centrifuge (TD5A-WS, Shanghai Jinghe Analytical Instrument Co., Ltd.) under the conditions of 4000 rpm for 15 min, then washed three times, dried, and stored in a sealed refrigerator.

2.2.2. Performance evaluation test method

The performance evaluation tests were conducted to investigate the effects of different factors, including adsorbent dosage, initial pH, contact time, and initial concentration, on the removal of chromium by nFeS-FA. The removal efficiency and adsorption capacity of Cr(VI) and total Cr were used as evaluation indicators to assess the impact of these factors. The control group was set by adding fly ash with a particle size of 120–150 mesh corresponding to the same weight to the wastewater. Three replicate experiments were performed for each group, the mean values were taken. The schematic representation of performance evaluation test is shown in Fig. 1.

2.2.2.1. The effect of adsorbent dosage. At 298.15 K, five portions of pre-prepared 200 mL wastewater containing 100 mg/L of Cr(VI) (pH = 4) were taken and treated with 2, 4, 6, 8, and 10 g/L of nFeS-FA, respectively. The mixture was stirred at 400 rpm for 150 min. After the completion of the experiment, samples were taken to measure the concentrations of Cr(VI) and total Cr. The calculation formula are as follows (1)(2).

$$\eta = \frac{C_0\text{-}C_t}{C_0} \times 100\% \tag{1}$$

$$q = \frac{(C_0\text{-}C_t) \times V}{m} \tag{2}$$

where: η is the removal efficiency, %; q is the adsorption capacity, mg/g; C_0 is the initial concentration, mg/L; C_t is the remaining concentration, mg/L; V is the volume of the solution, L; m is the mass of the nFeS-FA, g.

2.2.2.2. The effect of initial pH. At 298.15 K, five portions of pre-prepared 200 mL wastewater containing 100 mg/L of Cr(VI) were taken and treated with 8 g/L of nFeS-FA after adjusting their pH to 3, 4, 5, 6, and 7, respectively. The mixture was stirred at 400 rpm for 150 min. After the completion of the experiment, samples were taken to measure the concentrations of Cr(VI) and total Cr.

2.2.2.3. The effect of contact time. At 298.15 K, a pre-prepared 200 mL wastewater containing 100 mg/L of Cr(VI) (pH = 4) was taken and treated with 8 g/L of nFeS-FA. The mixture was stirred at 400 rpm for different contact times: 5, 10, 20, 30, 40, 50, 60, 90, 120, 150, and 180 min. After each specified contact time, samples were taken to measure the concentrations of Cr(VI) and total Cr.

2.2.2.4. The effect of initial concentration. At 298.15 K, five portions of pre-prepared 200 mL wastewater containing 60, 100, 140, 180, and 200 mg/L of Cr(VI) (pH = 4) were taken and treated with 8 g/L of nFeS-FA, respectively. The mixture was stirred at 400 rpm for 150 min. After the completion of the experiment, samples were taken to measure the concentrations of Cr(VI) and total Cr.

2.2.3. Adsorption isotherm and adsorption kinetics test method

Adsorption isotherm test: Solution with pH = 4, 200 mL, and different concentrations of Cr(VI) (initial concentrations were 60, 100, 140, 180, and 200 mg/L, respectively) were added into 250 mL conical flask. The solution was treated with 8 g/L of nFeS-FA. Stirring was conducted for 150 min at 298.15 K and 400 rpm. After the completion of the experiment, samples were taken to measure the remaining concentrations of Cr(VI) and total Cr in the solution. The experiment was conducted under optimal conditions. Three replicate experiments were performed for each group, the mean value was taken.

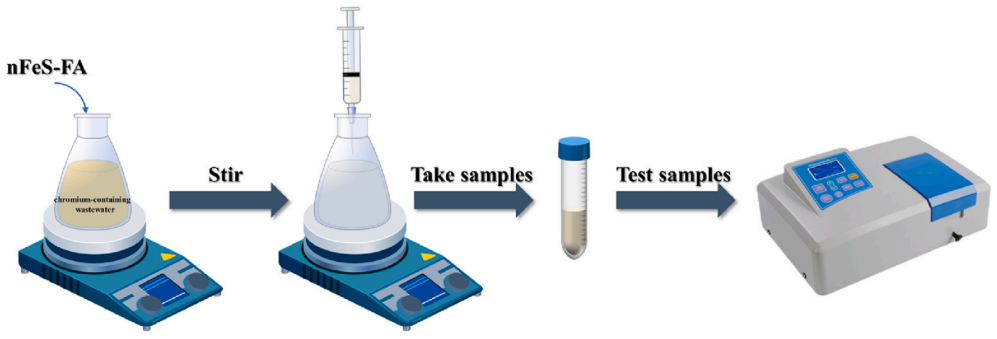

Fig. 1. Schematic representation of performance evaluation test.

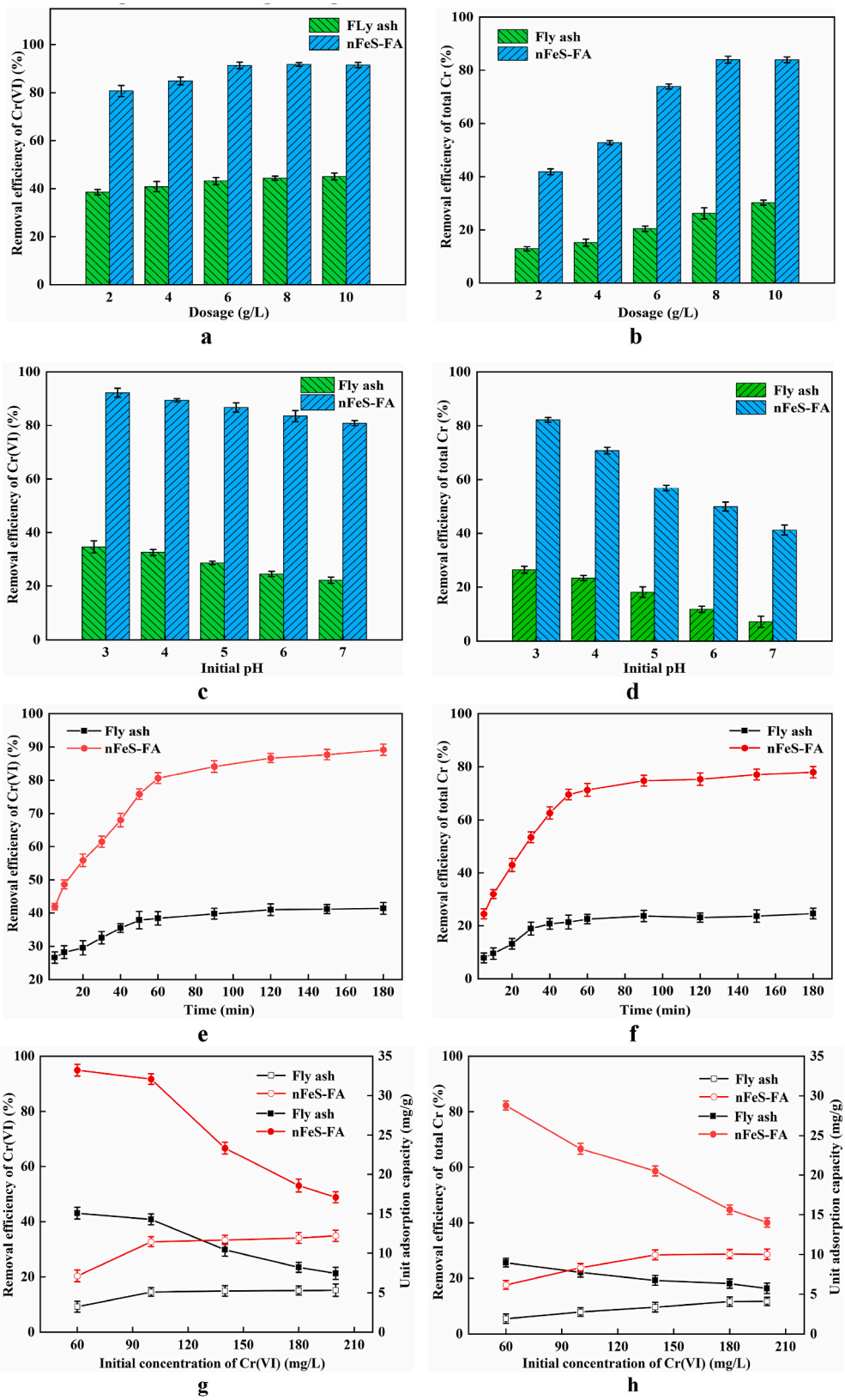

Fig. 2. The effect of adsorbent dosage, initial pH, contact time, and initial concentration on removal of Cr(VI) and total Cr.

Adsorption kinetics test: A solution with pH = 4 and Cr(VI) concentration of 100 mg/L was prepared, and 200 mL of the solution was added in a 250 mL conical flask. The solution was treated with 8 g/L of nFeS-FA. Stirring was conducted for 5, 10, 20, 30, 50, 60, 90, 120, and 150 min at 298.15 K and 400 rpm. After the completion of the experiment, samples were taken to measure the remaining concentrations of Cr(VI) and total Cr in the solution The experiment was conducted under optimal conditions. Three replicate experiments were performed for each group, the mean values were taken.

2.2.4. Water quality detection and material characterization method

Cr(VI) can be determined using the diphenylcarbazide spectrophotometric method (GB/T 7467–87). Total Cr can be measured using the potassium permanganate oxidation-diphenylcarbazide spectrophotometric method (GB/T 7466–87). pH can be measured using the glass electrode method (GB/T 6920–86).

X-ray diffraction (XRD, D8 ADVANCE, Bruker, Germany) was employed for the analysis of the mineralogical composition of the materials; Scanning electron microscopy and energy dispersive spectroscopy (SEM, SIGMA 500, Zeiss, Germany) was used to analyze the changes in the microscopic morphology and distribution of elements on the surface of materials; Transmission electron microscopy (TEM, Themis Z, FEI, USA) was used to analyze the morphological size. The specific surface area and pore size of the materials can be measured using the Brunauer, Emmett, and Teller (BET) method with Mack ASAP 2460 (Micromeritics Instrument Ltd., USA).

3. Results and analysis

3.1. The effect of adsorbent dosage

According to Fig. 2a, as the dosage of nFeS-FA increased, the removal efficiency of Cr(VI) gradually increased and then reached a stable level. Specifically, with an increase in dosage from 2.0 g/L to 8.0 g/L, the removal efficiency of Cr(VI) rapidly increased from 80.69 % to 91.75 %. Subsequently, as the dosage further increased from 8.0 g/L to 10.0 g/L, the removal efficiency of Cr(VI) reached a stable level. Similarly, according to Fig. 2b, the total Cr removal efficiency also exhibited a similar trend with increasing nFeS-FA dosage. The removal efficiency increased rapidly from 41.82 % to 83.97 % as the dosage increased from 2.0 g/L to 8.0 g/L, and then it tended to stabilize. However, as the dosage increased from 8.0 g/L to 10.0 g/L, the removal efficiency exhibited a slower increase and approached a relatively stable level. The removal of Cr(VI) and total Cr by nFeS-FA was much higher than that by fly ash, indicating that the loading nano-FeS effectively improved the reduction and immobilization of Cr(VI) and total Cr by fly ash. According to the above experiments, the removal efficiency of Cr(VI) and total Cr increased gradually. This is because with the increasing amount of adsorption materials, more adsorption sites for the adsorption of heavy metal ions are provided [29], and the removal efficiency of Cr(VI) and total Cr is greatly increased, and then tends to be stable because the adsorption has reached the equilibrium state. Therefore, in order to ensure the efficient removal of Cr(VI) and total Cr and save the amount of adsorbent, the amount of adsorbent was set to 8 g/L in subsequent experiments.

3.2. The effect of initial pH

According to Fig. 2c and d, with the increase of solution pH, the removal efficiency of Cr(VI) from nFeS-FA decreased gradually. When the solution pH increased from 3 to 7, the removal efficiency decreased from 92.20 % to 80.87 %. The removal efficiency of total Cr from nFeS-FA decreased rapidly with the increase of pH and decreased from 82.29 % to 41.25 % when the pH of the solution increased from 3 to 7. This is due to the higher solubility of FeS under acidic conditions, which can release more Fe^{2+} for rapid reduction of Cr(VI) [30]. At the same time, under acidic conditions, Cr(VI) mostly exists in $HCrO_4^-$ and CrO_4^{2-} states which are conducive to electrostatic adsorption, and are more conducive to rapid reduction by Fe^{2+} [31]. With the consumption of H^+ during the reaction, the solution pH gradually rose to neutral, and the Fe^{3+} generated by Fe^{2+} oxidation will generate hydroxide precipitation with Cr(III), so the removal capacity of nFeS-FA for Cr(VI) and total Cr will show a substantial increase compared with that of fly ash. Taking all factors into consideration, to ensure the efficient removal of Cr(VI) and total Cr, the initial pH for the subsequent experiments was set at 4.

3.3. The effect of contact time

According to Fig. 2e, when the contact time was from 5 min to 60 min, the removal efficiency of Cr(VI) increased rapidly, from 41.89 % to 80.64 %. When the contact time was from 60 min to 150 min, the removal efficiency increased from 80.64 % to 87.85 %, and the growth was slow, and tended to be stable. Fig. 2f showed that when the contact time was from 5 min to 60 min, the removal efficiency increased rapidly from 24.48 % to 71.31 %. When the contact time was from 60 min to 150 min, the removal efficiency increased from 71.31 % to 77.17 %, which increased slowly and tended to be stable. It can be seen from the above experiments that the removal efficiency of Cr(VI) and total Cr gradually increase and then tend to be stable. This is because a significant amount of FeS in the pores of nFeS-FA is involved in the adsorption process. As the contact time increases, the previously adsorbed heavy metal ions block the pores of nFeS-FA, hindering the adsorption process. Therefore, with an increase in contact time, there is no significant improvement in the removal efficiency of Cr(VI) and total Cr. Taking all these factors into consideration, to ensure the adsorption equilibrium, the contact time was set at 150 min for the subsequent experiments.

3.4. The effect of initial concentration

Fig. 2g and h, illustrated the relationship between the initial concentration of Cr(VI) and the corresponding removal efficiency and unit adsorption capacity. As the initial concentration of Cr(VI) varied, noticeable trends were observed. For the range of 60 mg/g to 100 mg/g, the removal efficiency of Cr(VI) exhibited negligible changes, with values decreasing from 94.92 % to 91.69 %. In contrast, the unit adsorption capacity experienced a significant increase, rising from 7.12 mg/g to 11.46 mg/g. Subsequently, as the initial concentration increased from 100 mg/g to 200 mg/g, a sharp decline in the removal efficiency was observed, dropping from 91.69 % to 48.83 %. However, the increase in unit adsorption capacity was relatively modest. Similarly, with an increase in the initial concentration of Cr(VI) from 60 mg/g to 140 mg/g, a substantial decrease in the removal efficiency of total Cr was observed, declining from 82.29 % to 58.58 %. Correspondingly, the unit adsorption capacity exhibited a significant increase from 6.17 mg/g to 9.95 mg/g. When the initial concentration further increased from 140 mg/g to 200 mg/g, the removal efficiency of total Cr experienced a rapid decline from 58.58 % to 40.09 %. In contrast, the increase in unit adsorption capacity was relatively small. It can be seen from the above experiments that at the beginning of the adsorption, nano-FeS can fully react with Cr(VI). With the increase of heavy metal ion concentration, the adsorption site of nFeS-FA was not enough to provide sufficient reaction site, so the removal efficiency decreased. In addition, the attachment of partial precipitation on the surface of nFeS-FA after the adsorption was not conducive to the reaction. Fly ash mainly relied on its porosity and large specific surface area to treat heavy metal wastewater, so its saturated adsorption capacity for pollutants was low [32]. Therefore, the initial concentration in the subsequent experiment was set to 100 mg/L.

3.5. Adsorption isotherms

The Langmuir, Freundlich adsorption isotherm model [33,34] were used to analyze the adsorption isotherms of nFeS-FA for Cr(VI) and total Cr. The linear expressions are as follows (3)–(4):

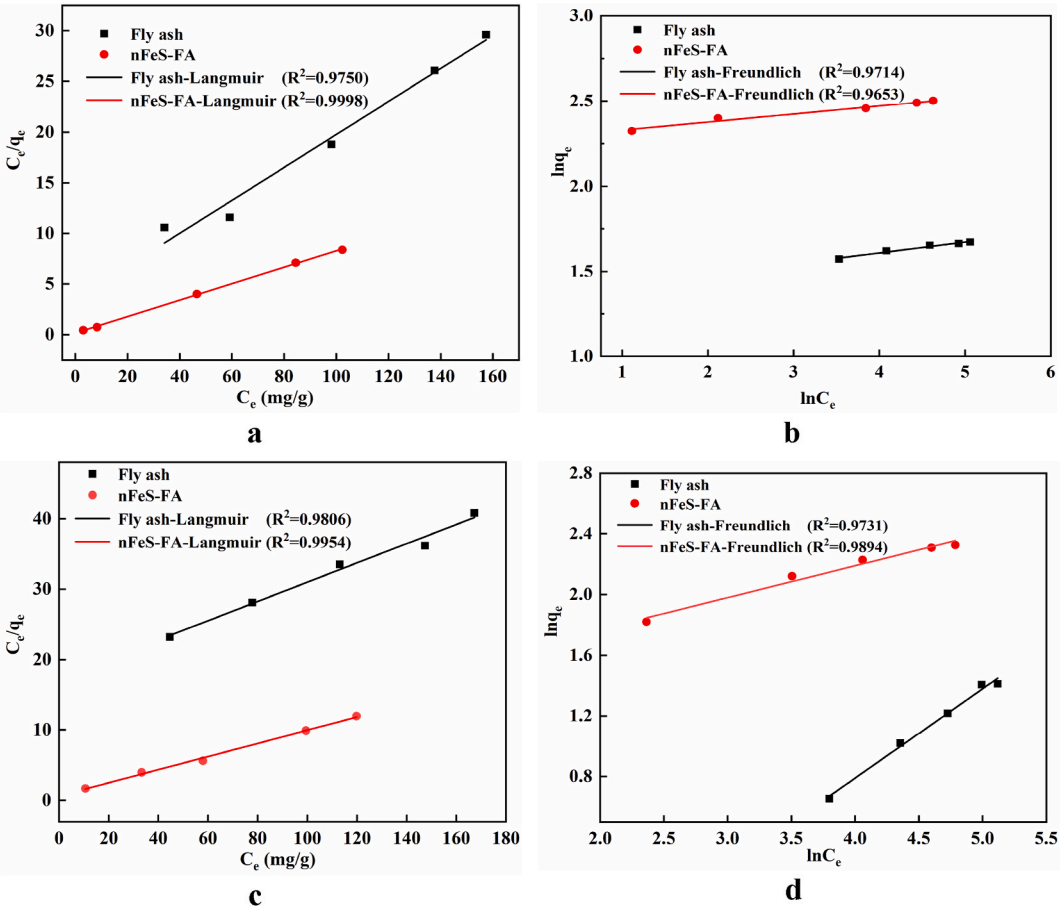

Fig. 3. The fitting diagram of isotherm model for adsorption of Cr(VI), total Cr by nFeS-FA. a: Langmuir model for Cr(VI), b: Freundlich model for Cr (VI), c: Langmuir model for total Cr, d: Freundlich model for total Cr.

$$\frac{C_e}{q_e}=\frac{1}{q_m K_L}+\frac{C_e}{q_m} \tag{3}$$

$$\ln q_e=\ln K_F+\frac{1}{n}\ln C_e \tag{4}$$

where, C_e is the pollutant concentration at solution equilibrium, mg/L; q_e is the adsorption capacity of adsorbent for pollutants at equilibrium, mg/g; q_m is the saturated adsorption capacity of the adsorbent for pollutants, mg/g; K_L is the Langmuir model adsorption constant; K_F is the Freundlich model adsorption constant; n is the Freundlich model adsorption strength correlation constant.

From Fig. 3a–d and Table 2, it was evident that the Langmuir isotherm model exhibited a higher linear correlation for the adsorption of Cr(VI) and total Cr by nFeS-FA. The fitted equations for the Langmuir curves were as follows: For Cr(VI): $C_e/q_e = 0.14088C_e + 0.08129$; For total Cr: $C_e/q_e = 0.67815C_e + 0.09285$. Therefore, nFeS-FA exhibited a monolayer adsorption mechanism for the adsorption of Cr(VI) and total Cr in the solution, which was found to be more fitting with the Langmuir model [35]. The correlation coefficients of adsorption strength, n, were all greater than 1, indicating that the adsorption was spontaneous [36]. As the adsorption sites became saturated gradually, the adsorption efficiency decreased gradually until it reached equilibrium. Compared with the saturated adsorption capacity q_m, it can be seen that nFeS-FA has a stronger adsorption capacity for Cr(VI) in solution. The Freundlich constants of Cr(VI) and total Cr were 0.04983 and 0.20964, respectively, and both were less than 0.5. This indicated that the adsorption process was relatively easy to occur. The magnitude of the Freundlich constant (K_F) is directly correlated and proportional to the adsorption capacity and intensity. The K_F values for Cr(VI) adsorption by fly ash and nFeS-FA were 3.8727 and 9.7872, respectively, while the K_F values for total Cr were 0.2083 and 3.8586, respectively. It showed that fly ash loaded nano-FeS can effectively improve the ability of fly ash to remediate wastewater containing Cr(VI). As shown in Table 3, when compared to several previously reported adsorbents, nFeS-FA exhibited superior adsorption performance.

3.6. Adsorption kinetics

The adsorption kinetics of Cr(VI) and total Cr by nFeS-FA were analyzed by using the pseudo-first order (PFO) kinetic model, the pseudo-second order (PSO) kinetic model, and intra-particle diffusion model [44,45]. The expressions used are as follows (5)–(7).

$$\mathrm{In}(q_e-q_t)=\mathrm{In}q_e-k_1 t \tag{5}$$

$$\frac{\mathrm{t}}{q_t}=\frac{1}{k_2 q_e^2}+\frac{\mathrm{t}}{q_e} \tag{6}$$

$$q_t=k_p \mathrm{t}^{1/2}+c \tag{7}$$

where: q_t is the adsorption capacity at the moment of adsorption t, mg/g; q_e is the equilibrium adsorption capacity, mg/g; k_1 is the adsorption rate constants for the PFO model, min; k_2 is the adsorption rate constants for the PSO model, mg/(g·min); k_p is the intraparticle diffusion rate constant, mg/(g·min$^{1/2}$); c is the boundary layer related parameter, mg/g.

Table 4 and Fig. 4a–d demonstrated that the PSO model exhibited a higher correlation coefficient compared to the PFO kinetic model for the adsorption of Cr(VI) by nFeS-FA. This suggests that the adsorption process for Cr(VI) by nFeS-FA predominantly followed the PSO model: $t/q_t = 0.0941t+1.0000$, $R^2 = 0.99872$, indicating chemisorption as the main mechanism. Similarly, the PSO model showed a higher correlation coefficient compared to the PFO model for the adsorption of total Cr by nFeS-FA. Consequently, the adsorption of total Cr by nFeS-FA was better described by the PSO model: $t/q_t = 0.0859t+0.9999$, $R^2 = 0.99763$, supporting chemisorption as the primary adsorption mechanism. The fitted curves of the intraparticle diffusion model for Cr(VI) and total Cr in Fig. 4e and f were not passed through the origin, indicating that the adsorption process was controlled by both adsorption mechanisms of film diffusion and intraparticle diffusion. nFeS-FA is a porous medium, and the adsorption of Cr(VI), total Cr from the liquid phase into nFeS-FA included three stages, indicating that the adsorption was a continuous segmentation process [46]. The first stage was mainly surface adsorption, where the diffusion of Cr(VI), total Cr from the solution to the outer surface of nFeS-FA occurred mainly in microvoids. The second stage was intraparticle diffusion, where Cr(VI) and total Cr were adsorbed onto the surface of nFeS-FA and then entered into the internal void. The third stage was the dynamic equilibrium stage of adsorption and desorption, and the diffusion rate

Table 2
Adsorption isotherm parameters of Cr(VI), total Cr by nFeS-FA and fly ash.

isotherm models	parameters	nFeS-FA		fly ash	
		Cr(VI)	total Cr	Cr(VI)	total Cr
Langmuir model	q_m	7.0982	1.4746	0.2851	0.0577
	K_L	1.7331	7.3037	21.5849	126.7773
	R^2	0.9998	0.9954	0.9750	0.98065
Freundlich model	n	21.07	4.77	15.71	1.70
	K_F	9.7872	3.8586	3.8727	0.2083
	R^2	0.9653	0.9894	0.9714	0.9731

Table 3
Comparison of adsorption properties of nFeS-FA with other adsorbents.

Adsorbents	pH	Dosage (g/L)	Equilibrium time (h)	Maximum adsorption capacity (mg/g)	References
modified zeolite supported zero-valent iron	7	20	2.5	2.49	[37]
humic acid coated magnetite nanoparticles	4	0.8	2	3.37	[38]
Fe@Fe_2O_3 core–shell nanowires	6.28	0.15	5	7.8	[39]
Nano-sized FeS-coated limestone	6.5	0.62	24	1.16	[40]
FeS-coated sand	4.7	100	72	2.75	[41]
Ball-milled Fe^0-biochar	5.5	2	72	14.6	[42]
Fe_3O_4@SiO_2/CTA-Br	3	12.5	1	3.38	[43]
nFeS-FA	4	8	2.5	12.21	This study

Table 4
Adsorption kinetics parameters of Cr(VI), total Cr by nFeS-FA and fly ash.

kinetic models	parameters	nFeS-FA		fly ash	
		Cr(VI)	total Cr	Cr(VI)	total Cr
PFO model	k_1	0.08114	0.04368	0.17155	0.05668
	q_e	10.1855	9.57685	4.88463	2.93626
	R^2	0.80564	0.95737	0.75816	0.97464
PSO model	k_2	8.8586×10^{-3}	7.3754×10^{-3}	9.4901×10^{-2}	3.4670×10^{-2}
	q_e	10.6247	11.6442	3.2461	5.3706
	R^2	0.99872	0.99763	0.99894	0.99816
intraparticle diffusion model	k_{p1}	0.7769	0.8073	0.1627	0.4113
	R^2	0.98724	0.9968	0.9487	0.9912
	C_1	3.5469	1.2796	2.9771	0.0476
	k_{p2}	1.0183	1.2616	0.3566	0.2992
	R^2	0.9795	0.9451	0.9712	0.8989
	C_2	2.6175	−0.4475	2.1284	0.6368
	k_{p3}	0.11093	0.1405	0.0673	0.0513
	R^2	0.91557	0.9337	0.8845	0.8741
	C_3	9.5618	7.8997	4.3181	2.3556

in this stage decreased and gradually reached the equilibrium state.

3.7. Characterization results

3.7.1. XRD analysis

The X-ray diffraction patterns of nFeS-FA before and after treating chromium-containing wastewater were shown in Fig. 5. Before the treatment, the characteristic diffraction peaks of quartz (PDF: #86–2237) appeared at $2\theta = 26.64°$, 50.14°, and 59.96°, and the characteristic diffraction peaks of mullite (PDF: #83–2465) appeared at $2\theta = 20.67°$ and 39.32° [47]. It indicated that the original characteristic diffraction peaks of fly ash loaded with FeS existed, and the crystal structure of fly ash had not been changed. The appearance of characteristic diffraction peaks of FeS (PDF:#76–0965) at $2\theta = 34.12°$ and 41.98° indicated the successful preparation of nFeS-FA, demonstrating the combination of nano-FeS with fly ash. The weak characteristic diffraction peaks of Fe_2O_3 (PDF: #85–0987) appeared at $2\theta = 20.70°$ and 33.34°, indicating that the prepared material has a small amount of oxidation. From the diffraction pattern of nFeS-FA after the treatment, it could be observed that the relative intensity of the characteristic diffraction peaks of mullite and quartz was weakened, which was due to the strong acid resistance of mullite, quartz, and other crystal phases, making them not easily dissolved [48]. Simultaneously, the characteristic peaks of nano-FeS disappeared, and a new diffraction peak appeared at $2\theta = 44.40°$, corresponding to the characteristic diffraction peak of FeOOH (PDF:#01–1223). New diffraction peaks appeared at $2\theta = 27.47°$, 34.18°, and 53.47°, corresponding to the characteristic diffraction peaks of Cr_2S_3 (PDF:#72–1224). It indicated that nFeS-FA reacted with Cr(VI) during the adsorption experiment, and the generated Fe^{3+} mostly precipitated in the form of FeOOH, while S^{2-} reacted with Cr(III) to produce Cr_2S_3 precipitation.

3.7.2. TEM analysis

From Fig. 6a and b, it can be observed that the flaky nano-FeS with a length distribution between 40 and 80 nm loaded on the surface of fly ash, which was nanoscale FeS. The nano-FeS on the nFeS-FA composite material shared similarities with the nano-FeS on FeS/Co_3S_4 synthesized by Deng et al. [49] (as shown in Fig. 6c), confirming the effective loading of nano-sized FeS onto fly ash using the ultrasonic precipitation method. Additionally, the nanoparticles exhibited good dispersion among themselves, confirming that using fly ash as a carrier material for the preparation of the composite material effectively addressed the aggregation of nano-sized FeS.

3.7.3. SEM-EDS analysis

To understand the surface microstructure of fly ash and nFeS-FA, scanning electron microscopy was used to observe the sample

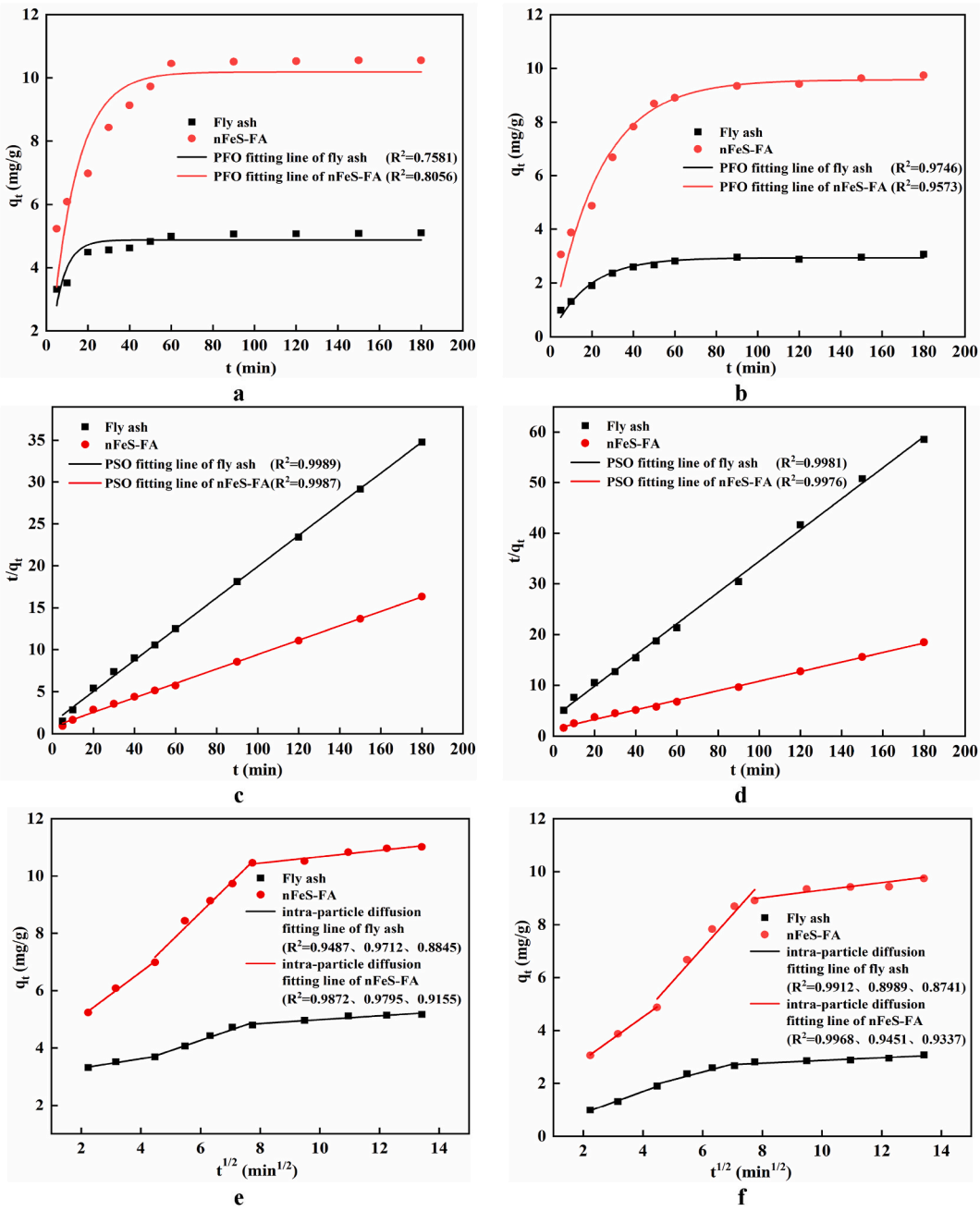

Fig. 4. The PFO model, the PSO model, and the intra-particle diffusion model for the adsorption of Cr(VI), total Cr by nFeS-FA. a: PFO fitting model of Cr(VI), b: PFO fitting model of total Cr, c: PSO fitting model of Cr(VI), d: PSO fitting model of total Cr, e: intra-particle diffusion model of Cr(VI), f: intra-particle diffusion model of total Cr.

surface, and the results were shown in Fig. 7 and Table 5. From Fig. 7a and b, the fly ash was spherical particles with smooth surface before the treatment, and these particles were mainly high-temperature silica-alumina droplets generated from the fly ash combustion process. After the treatment, the original smooth spherical shape of fly ash was broken, and the surface became rough and uneven. From Fig. 7c and d, it can be observed that the surface of nFeS-FA exhibited uniformly distributed flake-like nano-FeS crystals, with an overall fluffy appearance. This indicated that through ultrasonic precipitation treatment, nano-FeS has been efficiently loaded onto the surface of fly ash and exhibited good dispersion. After the treatment, the surface of nFeS-FA became concave, showing a loose cracked morphology and crystal precipitation appeared in the surface voids. The EDS spectra showed that the surface elements of fly ash and nFeS-FA were mainly Si, Al, and O. Combined with XRD analysis, these elements corresponded to the main crystalline phases of quartz and mullite in fly ash. Additionally, there was a small amount of C element, indicating the presence of incompletely combusted carbon

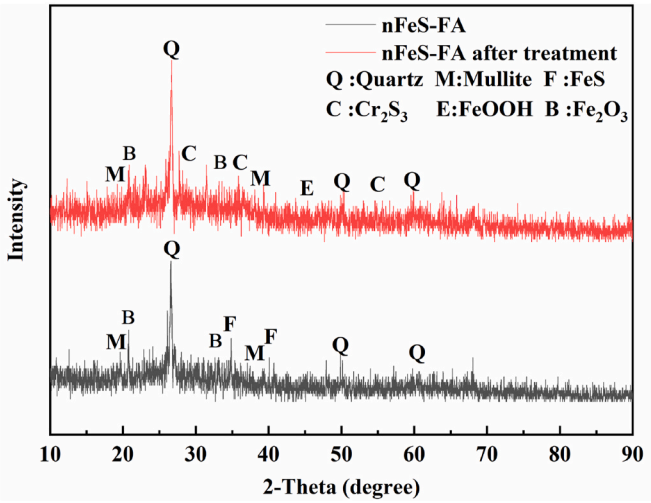

Fig. .5. X-ray diffraction patterns before and after treating chromium-containing wastewater by nFeS-FA.

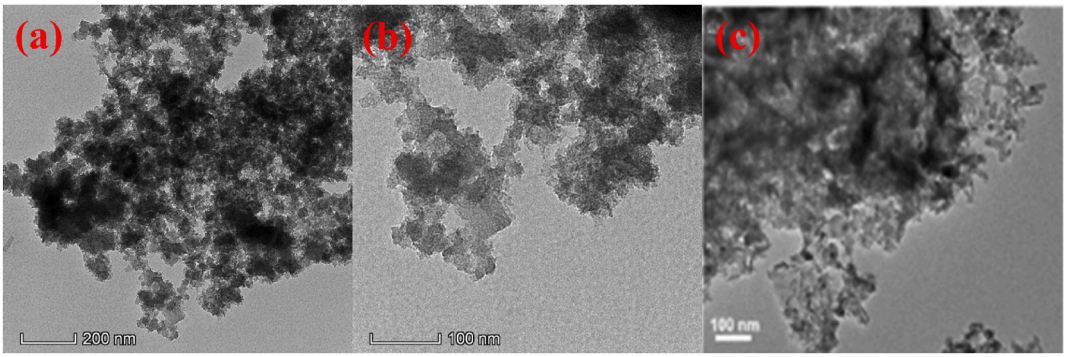

Fig. .6. TEM images. a–b: nFeS-FA, c: FeS/Co_3S_4 sample.

particles in fly ash. From Table 5, compared to fly ash, the mass percentage of Fe and S elements in nFeS-FA increased to 4.75 % and 2.73 % respectively, showing a significant increase. Combined with XRD and TEM analysis, it was further demonstrated that the successful preparation of nFeS-FA. Furthermore, after the treatment, the mass percentages of Cr element in fly ash and nFeS-FA were 0.12 % and 0.86 % respectively, indicating that both had a certain chromium fixation ability, and the adsorption performance of fly ash for chromium was enhanced after loading nano-FeS. Moreover, there was little change in the proportion of Fe element in nFeS-FA after treatment. This was because Fe^{2+} reacted with Cr(VI) to form Fe^{3+} through hydrolysis, resulting in the precipitation of FeOOH, and a small portion of Fe^{2+} oxidized to form Fe_2O_3, which adhered to the surface of nFeS-FA. However, the mass percentage of S element decreased, indicating that some S^{2-} combined with H^+ to form H_2S, which was released in gaseous form, while the remaining S^{2-} reacted with Cr(III) to produce Cr_2S_3 precipitation.

3.7.4. BET analysis

The specific surface area was related to the adsorption capacity of an adsorbent material. The results obtained from the calculations were shown in Table 6. Fig. 8 showed the N_2 adsorption-desorption isothermal curve of nFeS-FA, with the inset showing the BJH pore size distribution curve. The BET surface area and average pore volume of nFeS-FA were measured to be 12.16 m^2/g and 0.006266 cm^3/g, respectively, while those of fly ash were measured to be 4.38 m^2/g and 0.005140 cm^3/g, respectively. This could be attributed to the substantial removal of inorganic impurities from the fly ash during the synthesis of the material, which also led to the creation of a significant number of heterogeneous pores [50]. From Fig. 8, there were no noticeable differences observed in nFeS-FA at $P/P_0 < 0.5$, but distinct adsorption was observed in the range of 0.65–0.9. According to the classification of isotherm curves by Brunauer et al. [51], these curves belonged to Type IV. The hysteresis loop of H1-type in the pressure range of 0.65–1.0 indicated a uniform pore size and a relatively narrow pore size distribution. The pore size distribution graph revealed that the pores of the sample were primarily distributed around 3–8 nm, with an average pore size of 6.1788 nm, indicating that the prepared nFeS-FA was a mesoporous material. These results indicated that nFeS-FA synthesized by combining fly ash with nano-FeS effectively suppressed the aggregation of nano-FeS particles, resulting in the formation of thinner, more loosely dispersed nano-FeS, and increased its specific surface area.

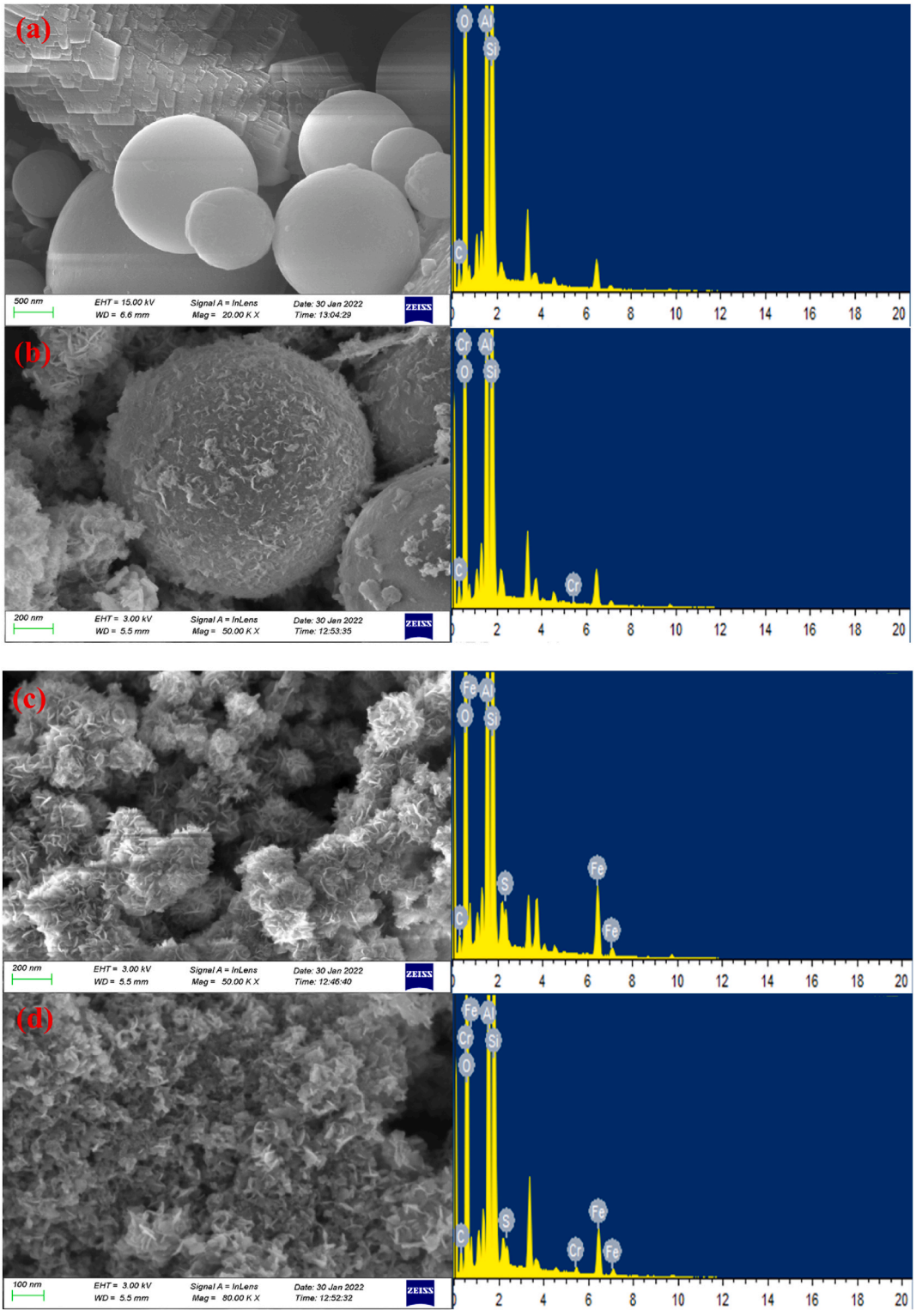

Fig. 7. SEM images and EDS spectra. a: Fly ash before the treatment, b: Fly ash after the treatment, c: nFeS-FA before the treatment, d: nFeS-FA after the treatment.

Table 5
The elemental composition before and after the treatment of fly ash and nFeS-FA.

Type	Element proportion/%						
	Si	Al	C	O	Fe	S	Cr
Fly ash before the treatment	25.05	10.65	1.11	63.19	0	0	0.00
Fly ash after the treatment	25.39	10.61	1.03	62.85	0	0	0.12
nFeS-FA before the treatment	23.30	10.02	1.06	58.50	4.75	2.73	0.00
nFeS-FA after the treatment	23.13	10.27	1.01	58.84	4.51	1.38	0.86

Table 6
Specific surface area and pore size of fly ash and nFeS-FA.

Type	Specific surface area (m^2/g)	Pore volume (cm^3/g)	Pore diameter (nm)
Fly ash	4.38	0.005140	5.2346
nFeS-FA	12.16	0.006266	6.1788

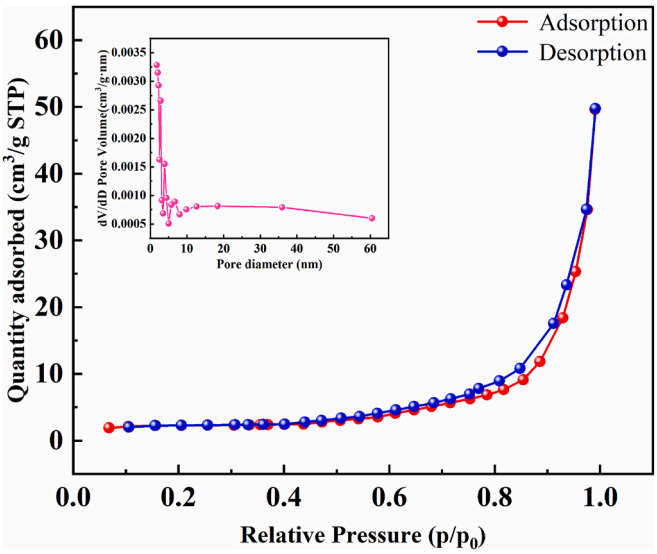

Fig. 8. The N_2 adsorption–desorption isotherm and Pore-aperture differential distribution curve of nFeS-FA.

Consequently, this was advantageous for the treatment of chromium-containing wastewater.

4. Conclusion

This study was based on the adsorption properties of fly ash and the reduction characteristics of nano-FeS. The nFeS-FA was prepared using mineral loading technology and ultrasonic precipitation method. It improved the mechanical strength and stability of nano-FeS, addressing the issue of nanoparticle aggregation, while also compensating for the low adsorption efficiency of fly ash alone, thereby enhancing the adsorption performance for chromium. Performance evaluation experiments showed that under optimal conditions, nFeS-FA achieved removal efficiency of 87.85 % for Cr(VI) and 71.77 % for total Cr, which were significantly higher than those of fly ash. The adsorption isotherm and adsorption kinetics fitting results showed that the adsorption of Cr(VI) and total Cr by nFeS-FA followed the Langmuir model and the pseudo-second-order kinetic model, indicating that the adsorption process was monolayer adsorption, mainly involved chemical adsorption. XRD, TEM, SEM-EDS, and BET revealed that the flaky nano-FeS with a length distribution between 40 and 80 nm was uniformly distributed on the surface of fly ash, exhibiting good dispersion and thereby increasing the specific surface area. During the adsorption experiments, nFeS-FA reacted with Cr(VI), and the generated Fe^{3+} mainly existed as FeOOH precipitation, while S^{2-} reacted with Cr(III) to produce Cr_2S_3 precipitation. This study demonstrated the potential application of nFeS-FA in treating acidic chromium-containing wastewater and also provided insights into the reuse of solid waste such as fly ash.

Ethics approval and consent to participate

Not applicable.

Availability of data and materials

Data will be made available on request.

CRediT authorship contribution statement

Xuying Guo: Writing – original draft, Validation, Methodology, Formal analysis, Conceptualization. **Zilong Zhao:** Writing – review & editing, Visualization, Software, Resources, Data curation. **Xinle Gao:** Supervision, Resources, Project administration. **Honglei Fu:** Validation, Supervision, Project administration. **Zhiyong Hu:** Writing – original draft, Investigation, Conceptualization. **Xiaoyue Zhang:** Supervision, Project administration, Investigation. **Yanrong Dong:** Supervision, Resources, Methodology, Conceptualization.

Declaration of competing interest

The authors declare that they have no known competing financial interests or personal relationships that could have appeared to influence the work reported in this paper.

Acknowledgments

The project is funded by the National Natural Science Foundation of China (51304114, 52304188), Department of Education of Liaoning Province (LJKFZ20220199), Science and Technology Department of Liaoning Province (2023-BS-201).

References

[1] F. Xia, Z. Zhao, X. Niu, Z. Wang, Integrated pollution analysis, pollution area identification and source apportionment of heavy metal contamination in agricultural soil, J. Hazard Mater. 465 (2024) 133215, https://doi.org/10.1016/j.jhazmat.2023.133215.
[2] W. Liu, J. Li, J. Zheng, Y. Song, Z. Shi, Z. Lin, L. Chai, Different pathways for Cr(III) oxidation: implications for Cr(VI) reoccurrence in reduced chromite ore processing residue, Environ. Sci. Technol. 19 (2020) 11971–11979, https://doi.org/10.1021/acs.est.0c01855.
[3] S. Shekhar Sarker, T. Akter, S. Parveen, Md Tushar Uddin, A. Kanti Mondal, S.M.A. Sujan, Microalgae-based green approach for effective chromium removal from tannery effluent: a review, Arab. J. Chem. 16 (2023) 105085, https://doi.org/10.1016/j.arabjc.2023.105085.
[4] J.G. Kim, J. Ku, J. Jung, Y.S. Park, G.H. Choi, S.S. Hwang, J.-H. Lee, A.S. Lee, Ion-exchangeable and sorptive reinforced membranes for efficient electrochemical removal of heavy metal ions in wastewater, J. Clean. Prod. 438 (2024) 140779, https://doi.org/10.1016/j.jclepro.2024.140779.
[5] N. Zhu, B. Zhang, Q. Yu, Genetic engineering-facilitated coassembly of synthetic bacterial cells and magnetic nanoparticles for efficient heavy metal removal, ACS Appl. Mater. Interfaces 12 (2020) 22948–22957, https://doi.org/10.1021/acsami.0c04512.
[6] Z. Xu, D. Li, Y. Tan, Q. Yang, H. Xiong, J. Li, H. Deng, Z. Lin, Investigation on the treatment of Cr(VI) by Bacillus cereus 12-2 under metal cation, Surface. Interfac. 24 (2021) 101141, https://doi.org/10.1016/j.surfin.2021.101141.
[7] E.M. Bakhsh, S.B. Khan, K. Akhtar, E.Y. Danish, T.M. Fagieh, C. Qiu, Y. Sun, V. Romanovski, X. Su, Simultaneous preparation of humic acid and mesoporous silica from municipal sludge and their adsorption properties for U(VI), Colloids. Surf. A. Physicochem Eng. Asp. 647 (2022) 129060, https://doi.org/10.1016/j.colsurfa.2022.129060.
[8] Z. Liu, M. Lei, W. Zeng, Y. Li, B. Li, D. Liu, C. Liu, Synthesis of magnetic Fe_3O_4@SiO^{2-}(-NH_2/-COOH) nanoparticles and their application for the removal of heavy metals from wastewater, Ceram. Int. 49 (2023) 20470–20479, https://doi.org/10.1016/j.ceramint.2023.03.177.
[9] W. Cao, D. Li, S. Zhang, J. Ren, X. Liu, X. Qi, Synthesis of hierarchical porous carbon sphere via crosslinking of tannic acid with Zn^{2+} for efficient adsorption of methylene blue, Arab. J. Chem. 16 (2023) 105122, https://doi.org/10.1016/j.arabjc.2023.105122.
[10] I. Matsukevich, Y. Lipai, V. Romanovski, Cu/MgO and Ni/MgO composite nanoparticles for fast, high-efficiency adsorption of aqueous lead(II) and chromium (III) ions, J. Mater. Sci. 56 (2021) 5031–5040, https://doi.org/10.1007/s10853-020-05593-4.
[11] Z. Xu, S. Gu, D. Rana, T. Matsuura, C.Q. Lan, Chemical precipitation enabled UF and MF filtration for lead removal, J. Water Process Eng. 41 (2021) 101987, https://doi.org/10.1016/j.jwpe.2021.101987.
[12] K.G.N. Quiton, Y.-H. Huang, M.-C. Lu, Recovery of cobalt and copper from single- and co-contaminated simulated electroplating wastewater via carbonate and hydroxide precipitation, Sustain. Environ. Res. 32 (2022) 31, https://doi.org/10.1186/s42834-022-00140-z.
[13] H. Wang, Y. Wang, Z. Liu, S. Luo, V. Romanovski, X. Huang, B. Czech, H. Sun, T. Li, Rational construction of micron-sized zero-valent iron/graphene composite for enhanced Cr(VI) removal from aqueous solution, J. Environ. Chem. Eng. 10 (2022) 109004, https://doi.org/10.1016/j.jece.2022.109004.
[14] M. Dai, J. Di, T. Zhang, T. Li, Y. Dong, S. Bao, S. Fu, Reparation of nano-FeS by ultrasonic precipitation for treatment of acidic chromium-containing wastewater, Sci. Rep. 14 (2024) 211, https://doi.org/10.1038/s41598-023-50070-y.
[15] G.P.W. Suyantara, H. Miki, D. Ochi, Y. Aoki, K. Ura, D. Berdakh, A. Ulmaszoda, E.P. Dwitama, K. Sasaki, T. Hirajima, Sodium metabisulfite as a copper depressant in the selective flotation of copper-molybdenum concentrate using seawater, Adv. Powder Technol. 34 (2023) 104258, https://doi.org/10.1016/j.apt.2023.104258.
[16] S. Fu, J. Di, X. Guo, Y. Dong, S. Bao, H. Li, Preparation of lignite-loaded nano-FeS and its performance for treating acid Cr(VI)-containing wastewater, Environ. Sci. Pollut. Res. 30 (2023) 3351–3366, https://doi.org/10.1007/s11356-022-22411-3.
[17] X. Guo, Z. Hu, X. Gao, Y. Dong, S. Fu, Study on the preparation of nano-FeS loaded on fly ash and its Cr removal performance, ACS Omega 7 (2022) 32331–32338, https://doi.org/10.1021/acsomega.2c03699.
[18] F. Hu, Y. Chen, Y. Hu, J. Chen, In-situ synthesis of Nano-FeS by sulfate reducting bacteria for Cr(VI)reduction, Environ. Prot. Chem. Ind. 42 (2022) 61–67, https://doi.org/10.3969/j.issn.1006-1878.2022.01.010 (in Chinese).
[19] Y. Li, W. Wang, L. Zhou, Y. Liu, Z.A. Mirza, X. Lin, Remediation of hexavalent chromium spiked soil by using synthesized iron sulfide particles, Chemosphere 169 (2017) 131–138, https://doi.org/10.1016/j.chemosphere.2016.11.060.
[20] H. Luo, F. Fu, B. Tang, Ferrous sulfide supported on modified diatomite for the removal of Cr(VI): performance and mechanism, Colloids. Surf. A. Physicochem Eng. Asp. (2023) 131538, https://doi.org/10.1016/j.colsurfa.2023.131538.
[21] Q. Li, Removal Mechanism of Hexavalent Chromium Using Biogenic Mackinawite (FeS)-Coating Kaolinite, South China University of Technology, Master Thesis, 2020, https://doi.org/10.27151/d.cnki.ghnlu.2020.004531 (in Chinese).

[22] X. Guo, X. Gao, S. Fu, G. Jiang, Y. Dong, Z. Hu, Dynamic experiment on the treatment of acidic chromium-containing wastewater by lignite loaded nano FeS, RSC Adv. 12 (2022) 6054–6062, https://doi.org/10.1039/D1RA08892K.
[23] V. Gadore, Md Ahmaruzzaman, Tailored fly ash materials: a recent progress of their properties and applications for remediation of organic and inorganic contaminants from water, J. Water Process Eng. 41 (2021) 101910, https://doi.org/10.1016/j.jwpe.2020.101910.
[24] L. Wang, X. Huang, J. Zhang, F. Wu, F. Liu, H. Zhao, X. Hu, X. Zhao, J. Li, X. Ju, P. Ji, Stabilization of lead in waste water and farmland soil using modified coal fly ash, J. Clean. Prod. 314 (2021) 127957, https://doi.org/10.1016/j.jclepro.2021.127957.
[25] W.x. Wang, Y. Qiao, T. Li, S. Liu, J. Zhou, H. Yao, H. Yang, M. Xu, Improved removal of Cr(VI) from aqueous solution using zeolite synthesized from coal fly ash via mechano-chemical treatment, Asia Pac. J. Chem. Eng. 12 (2017) 259–267, https://doi.org/10.1002/apj.2069.
[26] X. Deng, L. Qi, Y. Zhang, Experimental study on adsorption of hexavalent chromium with microwave-assisted alkali modified fly ash, Water Air Soil Pollut. 229 (2018) 18, https://doi.org/10.1007/s11270-017-3679-8.
[27] Z. Chen, Iron-based Nanomaterials Preparation and its Removal Mechanism for Uranium and Chromium in Water, Ph.D Thesis, North China Electric Power University (Bei jing), 2020, https://doi.org/10.27140/d.cnki.ghbbu.2020.000135 (in Chinese).
[28] S.M. Hosseini Asl, M. Masomi, M. Hosseini, H. Javadian, M. Ruiz, A.M. Sastre, Synthesis of hydrous iron oxide/aluminum hydroxide composite loaded on coal fly ash as an effective mesoporous and low-cost sorbent for Cr(VI) sorption: fuzzy logic modeling, Process, Saf. Environ. Prot. 107 (2017) 153–167, https://doi.org/10.1016/j.psep.2017.02.012.
[29] Y. Qiu, Q. Zhang, B. Gao, M. Li, Z. Fan, W. Sang, H. Hao, X. Wei, Removal mechanisms of Cr(VI) and Cr(III) by biochar supported nanosized zero-valent iron: synergy of adsorption, reduction and transformation, Environ. Pollut. 265 (2020) 115018, https://doi.org/10.1016/j.envpol.2020.115018.
[30] Y.-S. Han, H.J. Seong, C.-M. Chon, J.H. Park, I.-H. Nam, K. Yoo, J.S. Ahn, Interaction of Sb(III) with iron sulfide under anoxic conditions: similarities and differences compared to As(III) interactions, Chemosphere 195 (2018) 762–770, https://doi.org/10.1016/j.chemosphere.2017.12.133.
[31] Y. Zhang, L. Zhou, L. Chen, Y. Guo, F. Guo, J. Wu, B. Dai, Synthesis of zeolite Na-P1 from coal fly ash produced by gasification and its application as adsorbent for removal of Cr(VI) from water, Front. Chem. Sci. Eng. 15 (2021) 518–527, https://doi.org/10.1007/s11705-020-1926-9.
[32] X. Huang, H. Zhao, X. Hu, F. Liu, L. Wang, X. Zhao, P. Gao, P. Ji, Optimization of preparation technology for modified coal fly ash and its adsorption properties for Cd^{2+}, J. Hazard Mater. 392 (2020) 122461 https://doi.org/10.1016/j.jhazmat.2020.122461.
[33] G. Limousin, J.-P. Gaudet, L. Charlet, S. Szenknect, V. Barthès, M. Krimissa, Sorption isotherms: a review on physical bases, modeling and measurement, Appl. Geochem. 22 (2007) 249–275, https://doi.org/10.1016/j.apgeochem.2006.09.010.
[34] S. Yang, D. Zhao, H. Zhang, S. Lu, L. Chen, X. Yu, Impact of environmental conditions on the sorption behavior of Pb(II) in Na-bentonite suspensions, J. Hazard Mater. 183 (2010) 632–640, https://doi.org/10.1016/j.jhazmat.2010.07.072.
[35] X. Ma, W. Wang, C. Sun, H. Li, J. Sun, X. Liu, Adsorption performance and kinetic study of hierarchical porous Fe-based MOFs for toluene removal, Sci. Total Environ. 793 (2021) 148622, https://doi.org/10.1016/j.scitotenv.2021.148622.
[36] R.K. Mohapatra, P.K. Parhi, S. Pandey, B.K. Bindhani, H. Thatoi, C.R. Panda, Active and passive biosorption of Pb(II)using live and dead biomass of marine bacterium Bacillus xiamenensis PbRPSD202: kinetics and isotherm studies, J. Environ. Manag. 247 (2019) 121–134, https://doi.org/10.1016/j.jenvman.2019.06.073.
[37] H. Dang, Y. Zhang, P. Du, Enhanced removal of soluble Cr(VI) by using zero-valent iron composite supported by surfactant-modified zeolites, Water Sci. Technol. 70 (2014) 1398–1404, https://doi.org/10.2166/wst.2014.392.
[38] W. Jiang, Q. Cai, W. Xu, M. Yang, Y. Cai, D.D. Dionysiou, K.E. O'Shea, Cr(VI) adsorption and reduction by humic acid coated on magnetite, Environ. Sci. Technol. 48 (2014) 8078–8085, https://doi.org/10.1021/es405804m.
[39] Y. Mu, Z. Ai, L. Zhang, F. Song, Insight into core–shell dependent anoxic Cr(VI) removal with $Fe@Fe_2O_3$ nanowires: indispensable role of surface bound Fe(II), ACS Appl. Mater. Interfaces 7 (2015) 1997–2005, https://doi.org/10.1021/am507815t.
[40] L. Zhou, F. Dong, J. Liu, K.A. Hudson-Edwards, Coupling effect of Fe^{3+}(aq) and biological, nano-sized FeS-coated limestone on the removal of redox-sensitive contaminants (As, Sb and Cr): implications for in situ passive treatment of acid mine drainage, Appl. Geochem. 80 (2017) 102–111, https://doi.org/10.1016/j.apgeochem.2017.03.005.
[41] M. Park, J. Park, J. Kang, Y.-S. Han, H.Y. Jeong, Removal of hexavalent chromium using mackinawite (FeS)-coated sand, J. Hazard Mater. 360 (2018) 17–23, https://doi.org/10.1016/j.jhazmat.2018.07.086.
[42] K. Wang, Y. Sun, J. Tang, J. He, H. Sun, Aqueous Cr(VI) removal by a novel ball milled Fe^0-biochar composite: role of biochar electron transfer capacity under high pyrolysis temperature, Chemosphere 241 (2020) 125044, https://doi.org/10.1016/j.chemosphere.2019.125044.
[43] E.Z. Alharissa, Y. Efhiliana, R. Roto, M. Mudasir, E.T. Wahyuni, Efficient removal of Cr(VI) contaminant using recoverable silica from volcanic ash as natural adsorbent: synthesis and activity in the mechanism and kinetic adsorption, Heliyon 10 (2024) e23273, https://doi.org/10.1016/j.heliyon.2023.e23273.
[44] H. Yuh-Shan, Citation review of Lagergren kinetic rate equation on adsorption reactions, Scientometrics 59 (2004) 171–177, https://doi.org/10.1023/B:SCIE.0000013305.99473.cf.
[45] X. Guo, J. Wang, A general kinetic model for adsorption: theoretical analysis and modeling, J. Mol. Liq. 288 (2019) 111100, https://doi.org/10.1016/j.molliq.2019.111100.
[46] K.G. Akpomie, F.A. Dawodu, Efficient abstraction of nickel(II) and manganese(II) ions from solution onto an alkaline-modified montmorillonite, J. Taibah Univ. Sci. 8 (2014) 343–356, https://doi.org/10.1016/j.jtusci.2014.05.001.
[47] S. Gong, S. Feng, S. Wang, L. Yu, Y. Chen, Q. Xu, Strength and microstructural properties of silt soil cured by lime-activated fly ash-GGBS under different curing temperatures, Sci. Rep. 14 (2024) 6966, https://doi.org/10.1038/s41598-024-57741-4.
[48] P. Chindaprasirt, U. Rattanasak, Synthesis of porous alkali-activated materials for high-acidic wastewater treatment, J. Water Process Eng. 33 (2020) 101118, https://doi.org/10.1016/j.jwpe.2019.101118.
[49] S. Deng, X. Zhang, Y. Zhang, J. Ye, B. Mei, S. Lin, Flower-like iron sulfide/cobaltous sulfide heterostructure as advanced electrocatalyst for oxygen evolution reaction, Int. J. Hydrogen Energy 51 (2024) 550–557, https://doi.org/10.1016/j.ijhydene.2023.06.304.
[50] R. Xu, Q. Li, Y. Yang, S. Jin, L. Liao, Z. Wu, Z. Yin, B. Xu, X. Nan, Y. He, B. Zhu, T. Jiang, Removal of heavy metal(loid)s from aqueous solution by biogenic FeS-kaolin composite: behaviors and mechanisms, Chemosphere 299 (2022) 134382, https://doi.org/10.1016/j.chemosphere.2022.134382.
[51] S. Brunauer, L.S. Deming, W.E. Deming, E. Teller, On a Theory of the van der Waals Adsorption of Gases, J. Am. Chem. Soc. 62 (1940) 1723–1732, https://doi.org/10.1021/ja01864a025.